

Emission Control in Metal Halide Perovskite Lasers

Kaiyang Wang,[†] Can Huang,[†] Qifeng Ruan, Yu Zhou, Yimu Chen, Haoliang Liu, Shumin Xiao,* and Qinghai Song*



Cite This: *ACS Photonics* 2023, 10, 2091–2101



Read Online

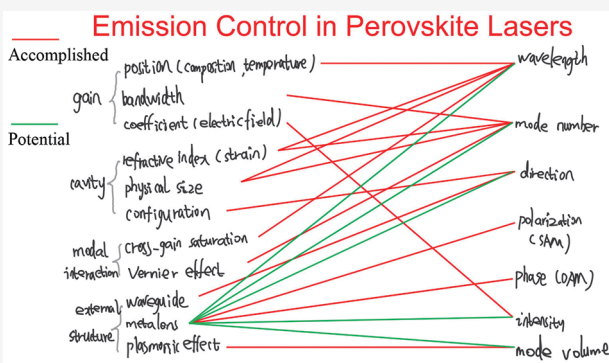
ACCESS |

Metrics & More

Article Recommendations

ABSTRACT: Metal halide perovskites, as promising photovoltaic materials, have shown great potential in coherent light sources due to their unprecedented properties, such as solution processability, low cost, large and balanced carrier mobility, high optical gain, and tunable bandgap. With the rapid development in the material synthesis and nanofabrication technique, perovskite lasers have been realized in a variety of compositions, morphologies, dimensions, sizes, excitation schemes, and cavity configurations, giving rise to distinct emission characteristics. In this perspective, the latest progress in the mode control over perovskite lasers, including emission wavelength, mode number, direction, polarization, and orbital angular momentum, is systematically reviewed. Criteria for evaluating the effectiveness of the strategies to steer the emission are proposed and discussed. Lastly, the challenges and trends for the mode control of perovskite lasers are presented.

KEYWORDS: Perovskites, lasers, mode control, microcavities, resonant nanostructures



INTRODUCTION

The past decade has witnessed booming development in the field of solar cells, enabled by the emerging semiconductors: metal halide perovskites. With a chemical formula of ABX_3 , perovskites possess rich chemical and structural diversities and exhibit superior properties, such as solution processability, easy and low-cost fabrication, long and balanced carrier diffusion length, high optical absorption coefficient, nice defect tolerance, etc. Up to now, the power conversion efficiency of perovskite based single-junction solar cells has increased from the initial 3.8% to 25.7%, approaching that based on crystalline silicon.^{1,2} Meanwhile, perovskites have also triggered great progress in light-emitting diodes,^{3–5} photodetectors,^{6–8} X-ray detectors,^{9–11} and lasers.^{12–14} As direct bandgap semiconductors, perovskites have shown high photoluminescence (PL) quantum yield, high optical gain coefficient, and tunable bandgap, thereby sparking extensive research attention in micro- and nanolasers.

Xing et al. observed amplified spontaneous emission (ASE) in perovskite thin films for the first time, which indicates the intrinsic suitability for coherent light emission.¹⁵ Since then, perovskite lasers have been demonstrated in versatile compositions (cations, anions), morphologies (films, wires, disks, spheres), crystalline phases (single crystal, multicrystal, quantum dot/well), sizes (nanoscale, microscale, millimeter scale), excitation schemes (pulsed, continuous-wave, single-photon, multiphoton), cavity configurations (vertical cavity surface emitting scheme, Fabry–Perot cavity, whispering

gallery mode cavity, photonic crystal cavity, distributed feedback cavity), etc. With the development in the material synthesis and fabrication/integration technique, lasing performance has been improved significantly, including low threshold ($\sim 220 \text{ nJ/cm}^2$),¹⁶ narrow line width ($< 0.1 \text{ nm}$),^{17–19} unidirectional emission,²⁰ small mode volume,^{21–23} vortex emission,^{24,25} and chiral emission.²⁶

Herein the latest progress in the emission control on perovskite lasers is systematically reviewed from the viewpoints of wavelength, mode number, direction, polarization, and orbital angular momentum. Critical benchmarks, involving compactness, uniformity, tunability, response time, and reproducibility, are introduced to evaluate the effectiveness of the strategies to steer the emission. To conclude, the challenges and trends in the emission control of perovskite lasers are presented.

EMISSION CONTROL METHODS

Wavelength Control. The optical bandgap of perovskites depends on the specific chemical compositions, which in turn

Special Issue: Photonics in China

Received: October 21, 2022

Revised: March 3, 2023

Accepted: March 6, 2023

Published: March 17, 2023



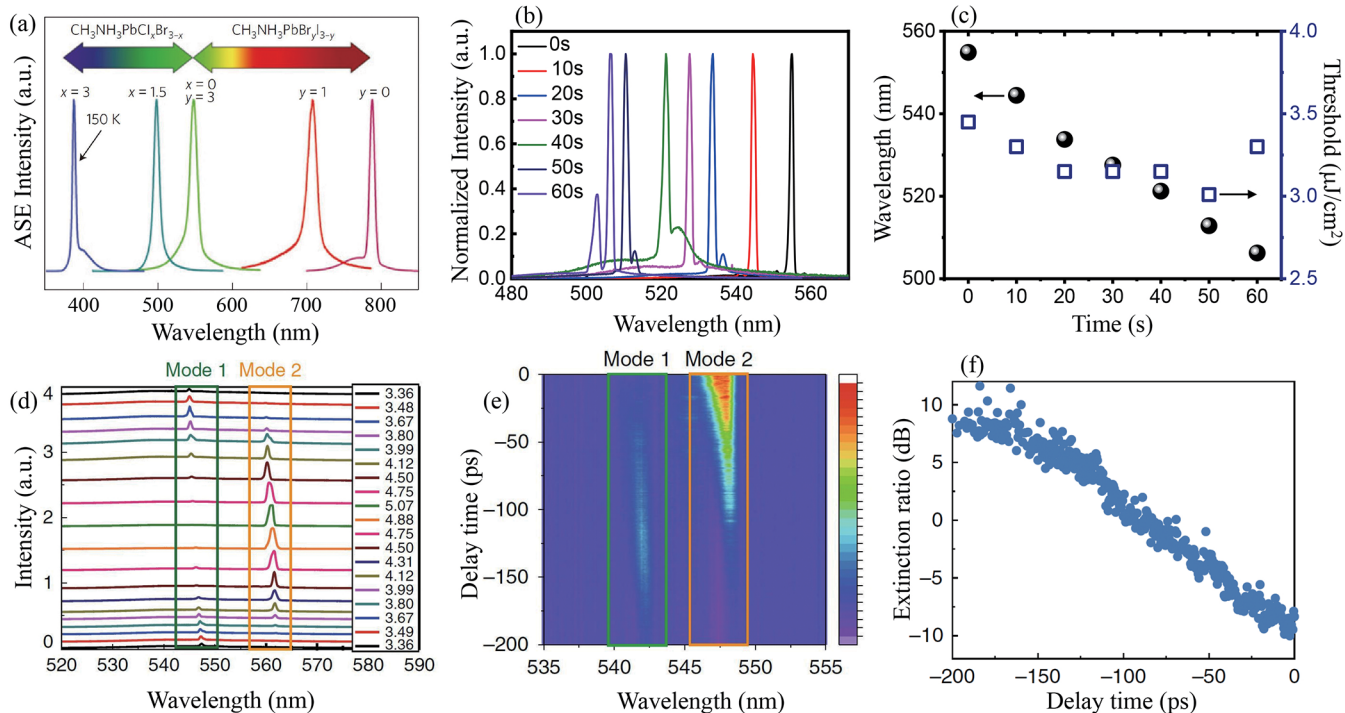


Figure 1. Wavelength control. (a) Broad ASE tunability from perovskite films with different halide composition. Reproduced with permission.¹⁵ Copyright 2014, Nature Publishing Group. (b) Lasing spectra evolution from a single-perovskite microwire with postsynthetic reaction time. (c) Lasing wavelength (spheres) and threshold (squares) of the perovskite microplate laser as a function of reaction time. (b, c) Reproduced with permission.³³ Copyright 2016, American Chemical Society. (d) The spectra evolution of lasing emission with the increase and decrease of pumping density. (e) Pseudocolor plot of the mode switching process with different delay times. (f) Extinction ratio between the two modes (mode-1/mode-2) as a function of delay time. (d–f) Reproduced with permission.³⁷ Copyright 2019, Nature Publishing Group.

determines the gain region. By mixing different halides in the precursor, Xing et al. demonstrated the continuous wavelength tunability of ASE ranging from 390 to 790 nm (see Figure 1a), which covers the entire visible spectra.¹⁵ In addition, the substitution of lead with tin extends the ASE peak wavelength to near-infrared (~950 nm).²⁷ Typically, the lasing wavelength distributes in the gain region and complies with the resonant condition of the cavity. By employing the naturally formed photonic crystal (PhC) cavity of a butterfly wing, the lasing wavelength of tin based perovskite exceeds 1 μm . Compared with the anion and divalent cation, the monovalent cation shows a much weaker influence on the bandgap, yet it affects the structural stability according to the Goldschmidt tolerance factor, which serves as a rule of thumb for predicting the formation and stability of a perovskite structure.²⁸ The ionic nature of perovskites makes it convenient and flexible to tune the bandgap via postsynthetic reactions in solid,²⁹ liquid,³⁰ and gas phases,³¹ which promises dynamic wavelength control. Although the morphology could be well preserved during the process of halide exchange, the emission capability degrades in most of the reported results.^{30,32} Zhang et al. reported dynamic and precise control over lasing wavelength from perovskite microstructures via postsynthetic reaction with chlorine.³³ Upon exposure to chloride in inductively coupled plasma (an etching machine), the bandgap of single-crystal CH₃NH₃PbBr₃ perovskite microstructures could be continuously tuned over 50 nm due to the halide exchange. As shown in Figure 1b, the lasing peak from a perovskite microwire shifts gradually from 555 to 503 nm as the reaction time increases to 60 s. Figure 1c summarizes the evolution of the emission wavelength as a function of reaction time, where the approximately linear

relationship allows precise control over the wavelength shift. More importantly, the lasing threshold shows a negligible change during the whole process, indicating the retention of crystal quality and emission capability. A heterojunction laser with dual color emission has also been demonstrated in a single-perovskite microplate by site-selective halide substitution. The lack of a proper gas containing bromide and iodine sets a limit on the tuning range and shift direction of the lasing wavelength. By taking advantage of the intrinsic dependence of bandgap on temperature, Xing et al. observed a redshift of the lasing wavelength with decreasing temperature and sudden hopping at the phase transition point.³⁴

Besides engineering the material bandgap, the external stimuli that affect the physical parameters of resonant cavities will also induce a wavelength shift. Yang et al. transferred perovskite nanowires to flexible substrate and achieved dynamic tuning of the lasing wavelength by applying compressive or tensile strain, which has been ascribed to the piezoelectric polarization effect induced refractive index change of the nanowires.³⁵ Inspired by the wide-band tunability of liquid crystal (LC) lasers, Chen et al. constructed perovskite quantum dot doped lasers with planar cholesteric liquid crystal cavities and realized continuous tuning of the lasing wavelength based on the shift of photonic bandgaps under thermal or electrical stimuli.³⁶ However, the lasing intensity drops dramatically and even ceases during the regulation process. Zhang et al. proposed and demonstrated a robust mechanism to realize all-optical control on the lasing wavelength of perovskites.³⁷ As shown in Figure 1d, as the pump fluence increases, the initial lasing mode (left peak) with lower threshold is switched off by the second mode (right peak).

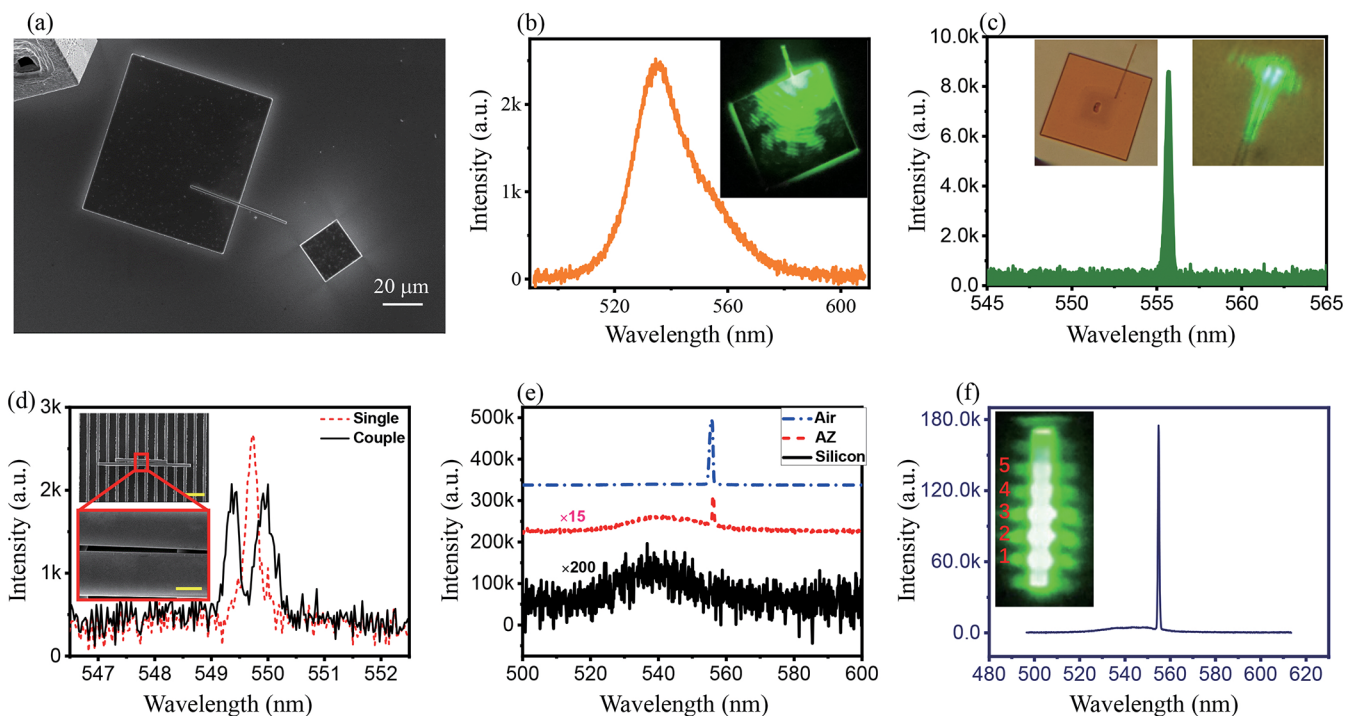


Figure 2. Mode number control. (a) Top-view SEM of the microwire on perovskite microplate with one end suspended in air. (b) Fluorescence spectrum of the fully pumped microwire. The inset shows the fluorescence image of the microwire. (c) Single-mode emission from the suspending part of a $\text{CH}_3\text{NH}_3\text{PbBr}_3$ microrod. The insets show the optical and fluorescence images. (a–c) Reproduced with permission.⁵³ Copyright 2016, Optical Society of America. (d) Lasing spectrum from a photonic molecule laser, where the insets are top-view SEM images with scale bars of 10 and 1 μm . Reproduced with permission.⁵⁴ Copyright 2017, Wiley-VCH. (e) Emission spectra from a single-perovskite microwire under the same pump fluence on different substrates where AZ stands for the photoresist. (f) Lasing spectrum of a microwire that is entirely pumped. The inset is the corresponding fluorescent microscope image. (e, f) Reproduced with permission.⁵⁵ Copyright 2016, American Chemical Society.

Interestingly, the mode switching process is reversible by controlling the pump fluence. The underlying mechanism is explained by the cross-gain saturation induced nonlinear modal interactions.³⁸ The switching time is investigated based on a self-built double pump scheme, and the experimental results are shown in Figure 1e,f. The switching time is determined to be 75 ps by defining a 10 dB extinction ratio as a standard. The dynamic, reversible, ultrafast, all-optical control over the lasing modes is suitable for other laser systems and shall shed light on the potential applications including optical memories and flip-flops. Wavelength control is oriented to tunable lasers and thus should meet the requirements on tuning range, dynamic control, and output stability. Stoichiometric engineering, especially on halide composition, allows broad wavelength tunability, yet it impedes practical application due to failure in postsynthetic and dynamic control. Although direct modulation on perovskites via external stimuli, including temperature, strain, and electrical bias, could offer fine-tuning on the emission wavelength, irreversible degradation will be imposed on perovskite materials during the tuning process, which affects the reproducibility and stability. All-optical control based on modal interaction promises ultrafast and dynamic control between the two lasing modes.³⁷ However, it lacks continuous tunability over wavelength. An external cavity laser, composed of perovskite heterostructures³⁹ (broadband coherent light source) and an external resonant cavity⁴⁰ (wavelength-selective and stimuli-responsive component), is a promising alternative to realize broadband, dynamic, and reproducible tunable lasers.

Mode Number Control. For lasers, the emission characteristics, such as line width, lifetime, wavelength, mode

number, direction, polarization, etc., are closely related to the three basic elements, specifically gain material, pump source, and resonant cavity. In particular, the mode number of perovskite lasers shows a positive correlation with the resonant cavity size, which is mediated by the inverse proportional dependence of mode spacing on the cavity length. Following the canonical route, single-mode lasing emission has been first observed in vertical cavity surface emitting cavities,^{41,42} photonic crystal cavities,^{43–45} and distributed feedback (DFB) cavities^{46–48} owing to the greatly reduced cavity length. Take the vertical cavity surface emitting laser (VCSEL) as an example. Distributed Bragg reflectors or metal mirrors are utilized to confine the emitted light from the gain medium, which is sandwiched between the two reflectors. The channel gap between the bottom and top reflectors defines the physical size of the vertical Fabry–Perot (FP) cavity. Typically, the thickness of the gain medium is on the subwavelength scale and the corresponding free spectral range (mode spacing between two consecutive resonant modes) is much larger than the gain bandwidth, thus resulting in single-mode emission.^{41,42,49} Also the lasing wavelength and mode number of VCSEL can be tuned by the thickness of the gain medium. Wang et al. investigated the resonant cavity induced modulation on the spontaneous emission systematically and demonstrated multimode lasing emission from perovskite quantum dot based VCSEL.⁵⁰ For individual perovskite microstructures, which function as a resonant cavity and gain material simultaneously, single-mode lasing emission has been realized in microdisks,⁵¹ nanowires,¹⁶ and microspheres⁵² with subwavelength-scale size. In addition to the common cavities,

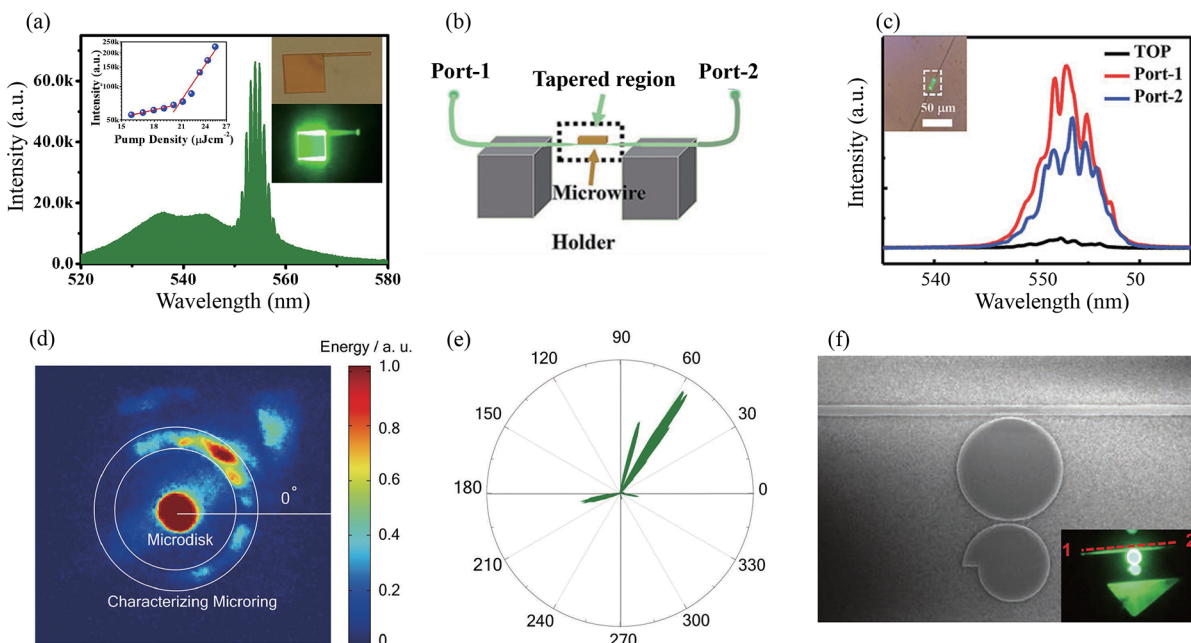


Figure 3. Emission direction control. (a) The WGM lasing spectrum from the waveguide connected perovskite microdisk where the insets show the optical and fluorescence microscope images. (a) Reproduced with permission.²⁰ Copyright 2016, American Chemical Society. (b) The scheme of a hybrid system of perovskite nanowire and tapered fiber. (c) Lasing emission spectra collected from the objective (top) and tapered fiber (port) where the inset shows the fluorescence microscope image above the lasing threshold. (b, c) Reproduced with permission.⁷⁴ Copyright 2016, Royal Society of Chemistry. (d) Fluorescence microscope image of the device demonstrating directional emission. (e) Numerically calculated far-field pattern. (d, e) Reproduced with permission.¹⁸ Copyright 2017, Wiley-VCH. (f) The top-view SEM image of the fabricated waveguide–photonic molecule system, where the scale bar is 10 μm . The inset shows the corresponding fluorescence microscope image pumped above threshold. (f) Reproduced with permission.⁷⁸ Copyright 2018, Wiley-VCH.

such as the FP cavity in micro- and nanowires and the whispering gallery (WG) cavity in polygonal microdisks/microplates and microspheres, Wang et al. reported a transverse WG mode in the cross-sectional plane of perovskite microwires.⁵³ As shown in Figure 2a, leaky loss is introduced to one end of the microwire by suspending it on a homogeneous substrate (perovskite microplate) to get rid of the competition with the FP mode along the axial direction. Under full pump on the whole microwire, only strong fluorescence is observed (see Figure 2b). However, by moving the pump spot to the suspending end of the microwire, single-mode lasing emission is observed, as illustrated in Figure 2c. The cross-sectional plane of the perovskite microwire supports two possible resonant modes: the transverse FP mode and the transverse WG mode. The cubic phase of single-crystal $\text{CH}_3\text{NH}_3\text{PbBr}_3$ perovskite microwires leads to approximately square cross sections. In such a case, the transverse WG mode possesses a much higher quality factor and thus dominates the output lasing mode. On the basis of the transverse WG mode, Wang et al. demonstrated homonuclear photonic molecule lasers consisting of two evanescently coupled perovskite microwires.⁵⁴ As shown in Figure 2d, single-mode emission from an individual microwire splits into the antibonding mode and the bonding mode in the coupled system. Furthermore, the transverse WG mode lasing action is applied to realize a high-density and uniform nanolaser array.⁵⁵ Figure 2e shows the emission spectra evolution from the same perovskite microwire on three common substrates with different refractive indexes, suggesting the crucial role of leaky loss in output emission. By leveraging the distinctive emission characteristics on silicon substrate versus in the air, a nanolaser array is demonstrated in a perovskite microwire suspending on a

silicon grating (see Figure 2f). Benefiting from the high crystal quality of perovskite microwire, different segments possess nearly the same cavity size and gain profile, promising uniform lasing emission. The integration density of the nanolaser array depends on the grating periodicity and eventually is subjected to the diffraction limit. The Vernier effect and inverse Vernier effect between coupled lasing cavities have been widely utilized to achieve single-mode emission.^{56–61} Li et al. fabricated coupled FP cavities by cutting perovskite microwire into two segments via the focused ion beam milling approach and demonstrated single-mode lasing emission.⁶² Individual perovskite micro- and nanostructures on the wavelength scale, including nanowires,^{16,53} microspheres,⁵² and micro- and nanocubes,^{63,64} are potential candidates for compact, miniaturized, single-mode lasers. However, the random size distribution of chemically synthesized perovskites sets a limit on the precise control over wavelength and reproducibility. In comparison, integration of perovskites with external resonant cavities or directly patterning artificial nanostructures on perovskites ensures single-mode emission with good reproducibility.^{65–69} However, care must also be taken in dealing with scalable fabrication, time cost, complexity, and uniformity.

Emission Direction Control. The far-field direction of lasing emission is typically dictated by the cavity configuration. For micro- and nanowires, the FP mode lasing emits in two directions at the two end facets, whereas square microplates with a dominant WG mode emit in four directions from the corners. The rotation symmetry of the circular microdisk causes isotropic emission, which severely impedes the utilization efficiency. VCSEL possesses intrinsic merit in unidirectional emission. In contrast, a random laser, based on a complex and mirrorless cavity, exhibits arbitrary emission

patterns, which originates from interference among multiple scattered waves.⁷⁰ Liu et al. implemented a surface emitting random laser by sandwiching perovskite polycrystalline film between two distributed Bragg reflectors and achieved directional lasing emission.⁷¹ In the DFB cavity, the emission direction follows the Bragg conditions, $m\lambda_{\text{Bragg}} = 2n_{\text{eff}}\Lambda$, where m is the Bragg order, λ_{Bragg} is the Bragg wavelength, n_{eff} is the effective refractive index taking the environment and resonant structure into account, and Λ is the grating periodicity: edge emitting mode for $m = 1$ and surface emitting mode for $m = 2$. Zhizhchenko et al. imprinted a nanograting on the surface of perovskite microwire and realized directional emission in the vertical direction.⁷² Wang et al. developed a chemical synthesis method and obtained a perovskite based waveguide connected microdisk.²⁰ As shown in Figure 3a, the joint point lies at the corner of the square microdisk, which has negligible perturbation on the electromagnetic field distribution of the WG mode in the microdisk. Owing to the homogeneous connection, the lasing emission from the perovskite microdisk transports through the waveguide channel, thereby forming unidirectional output emission. Similarly, Trofimov et al. embedded a gallium phosphide nanowire in the perovskite microstructure and guided the lasing emission via the nanowire.⁷³ To increase the collection efficiency, Gu et al. utilized tapered fiber instead of an objective to collect the lasing emission from perovskite microwires.⁷⁴ As depicted in Figure 3b, the perovskite microwire adhered to the tapered fiber via van der Waals force and the laser emission coupled to and propagated along the fiber. The collection efficiency improved over an order of magnitude compared with that via the objective with a high numerical aperture (see Figure 3c). To boost the collection efficiency of the WG mode lasing emission, Cegielski et al. integrated perovskite microdisk lasers with a silicon nitride waveguide via evanescent coupling.^{75,76} Based on a CMOS compatible manufacturing technique, Zhang et al. fabricated a deformed microdisk on a perovskite microplate and achieved efficient control on the emission direction.¹⁸ Although the ray dynamics is mostly chaotic, the resonant mode with a relatively high quality factor, which is formed by wave localization along the unstable periodic ray trajectories, will emit out along one direction due to the presence of unstable manifolds in the chaotic sea.⁷⁷ Figure 3d illustrates the far-field emission pattern of a perovskite deformed microdisk, which is consistent with the numerical simulation result (see Figure 3e). Then Wang et al. proposed a compound structure made of a waveguide coupled photonic molecule and demonstrated unidirectional lasing emission by breaking the symmetry between clockwise and counter-clockwise components.⁷⁸ As shown in Figure 3f, the circular microdisk evanescently coupled simultaneously to a straight bus waveguide and a spiral cavity defined in polar coordinates as $\rho(\theta) = R(1 + \varepsilon\theta/2\pi)$, where R and ε denote the radius and deformation parameter, respectively. Under an optical pump, directional emission along the waveguide to the left end can be clearly observed in the fluorescence microscope image. The emission direction is closely related to the utilization efficiency of the perovskite laser. For free space application, the vertical cavity surface emitting scheme possesses intrinsic advantages over other cavity configurations, including compactness, low divergence angle, and circular beam profile. As for on-chip applications, the waveguide connected scheme ensures maximum utilization efficiency. However, design optimization over the relative position, width, and material selection of the

waveguide should be carried out to suppress the perturbation on the original resonant modes and to maximize the collection efficiency simultaneously.

Polarization Control. As an intrinsic merit of lasing emission, polarization describes the variation of output intensity as a function of angles. The lasing polarization becomes complicated for three-dimensional resonant cavities as a result of complex mode distribution.^{23,63,64} For a vertical cavity surface emitting laser and random laser, the polarization is also hard to define. Therefore, we focus our attention on the polarization characteristics from simple one-dimensional and two-dimensional perovskite lasers. For FP mode lasing supported in perovskite micro- and nanowires, the polarization is detected in the plane parallel to the substrate and transverse electric (magnetic) polarization is defined as the dominant electric (magnetic) field polarized perpendicular to the long axis of the micro- and nanowires; for WG mode lasing in perovskite microplates or microdisks, polarization is detected in the plane perpendicular to the substrate and transverse electric (magnetic) polarization is defined as the dominant electric (magnetic) field polarized parallel to the substrate plane; for DFB lasers, the polarization is detected in the plane parallel to the substrate and transverse electric (magnetic) polarization is defined as the dominant electric (magnetic) field polarized parallel to the grating grooves. The polarization of these three kinds of perovskite lasers is fundamentally determined by the waveguide mode which they coupled to. Generally, to realize laser emission, the perovskite based lasing cavity is placed on a substrate with a relatively small refractive index, which ensures the formation of a waveguide mode. For the transverse electric polarized mode, the electromagnetic field mainly distributes in perovskite and experiences less leaky loss. Therefore, perovskite lasers based on the above-mentioned three resonant cavities exhibit linear polarization with the transverse electric mode.^{16,46,79,80} For perovskite PhC lasers based on the photonic band-edge mode, isotropic polarization dominates for the Γ -point mode whereas anisotropic polarization dominates for the M- and X-point modes.^{44,45} Dai et al. reported the first circularly polarized lasing emission by integrating the perovskite microwire laser with a metalens.²⁶ The perovskite microwire laser is placed at the focal point of the metalens and serves as a point source with linear polarization, which in principle can be decomposed into two circularly polarized components. The metalens is designed based on the Pancharatnam–Berry phase and works as a convex (concave) lens for the incident plane wave with left (right) circular polarization. Following the time-reversal process, the decomposed left (right) circularly polarized component is collimated (diverged) into a right (left) circularly polarized beam. Hence, a highly directional lasing emission with pure right circular polarization is demonstrated. In addition, the dependence of emission intensity on excitation polarization has been studied and emission anisotropy with a maximum polarization ratio up to 0.78 is demonstrated in ultrathin perovskite nanowires due to the dielectric mismatch between the high dielectric nanowires and the surrounding air.⁸¹ Furthermore, taking advantage of the excitation polarization dependent gain coefficient in the single-crystal perovskite microplate with anisotropic orthorhombic phases, all-optical switching of lasing emission has been realized.⁸² Polarization control in perovskite lasers, especially circularly polarized emission, is still in the early stages and needs more research attention. Upon introducing the concept of a

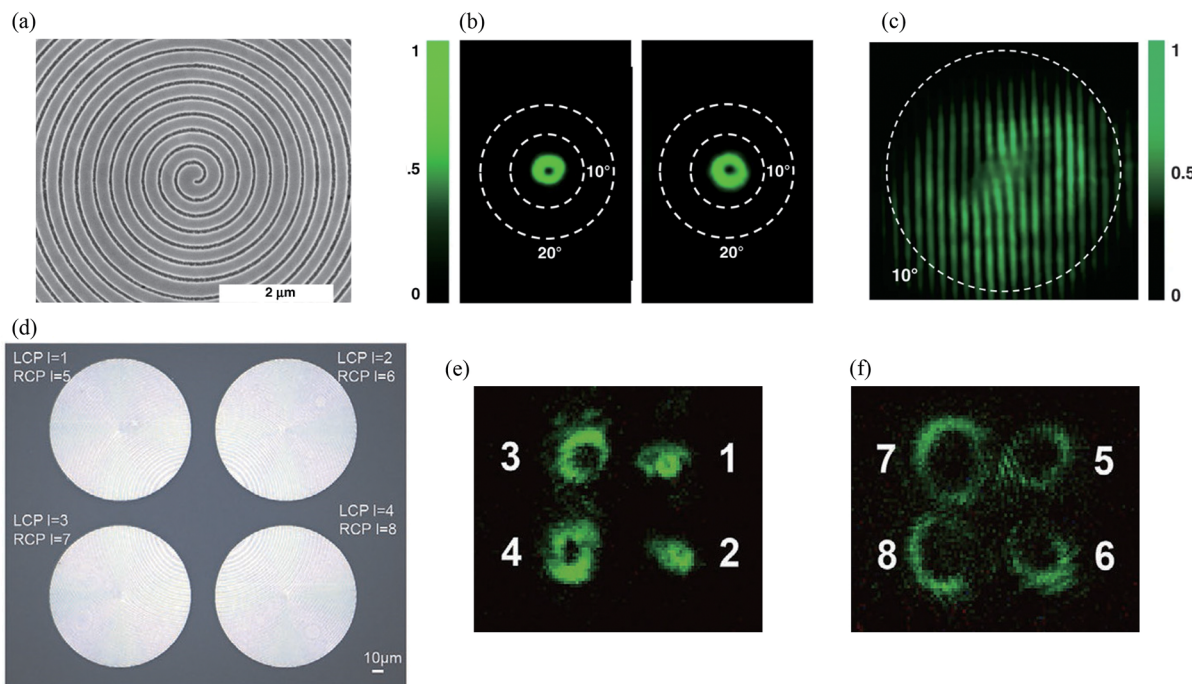


Figure 4. Wavefront control. (a) Top-view SEM image of the perovskite Archimedean spiral grating. (b) Far-field laser emission profiles in the forward direction and backward direction. (c) Measured self-interference pattern of the laser beams in the forward direction. (a–c) Reproduced with permission.²⁴ Copyright 2020, Nature Publishing Group. (d) The top-view optical microscopy image of the metalens array. (e, f) The far-field collected beam profiles by placing a perovskite microlaser at the focal spot where (e) and (f) correspond to the LCP and RCP polarization states, respectively. (d–f) Reproduced with permission.²⁵ Copyright 2022, Wiley-VCH.

metasurface into perovskite structures, chiral spontaneous emission from perovskites has been reported by several research groups.^{83–85} Circularly polarized lasing emission with large chirality and high quality factor⁸⁶ shall be explored in a perovskite system in the future.

Wavefront Control. The left or right circular polarization of the light beam corresponds to the spin angular momentum of the photons. In fact, photons also possess orbital angular momentum (OAM), which corresponds to the spiral distribution of the wavefront. The light beam rotates around its optical axis in space during propagation, forming a vortex beam, and the order of OAM is defined by the number of windings in one period.⁸⁷

Vortex beams can be generated via spatial light modulator, spiral phase plate, computer-generated hologram, metasurface, etc.⁸⁸ Sun et al. experimentally fabricated high-quality grating structures on perovskite thin films and obtained a VCSEL with a divergence angle of 3° .²⁴ Via introducing an Archimedean spiral grating (see Figure 4a), the wavefront of the perovskite VCSEL transforms to a spiral wave with topological charge from -4 to $+4$, showing highly directional output and well controlled topological charge, as shown in Figure 4b,c. Additionally, Zhang et al. reported a vortex laser array by integrating a perovskite microwire with a metalens array, where an individual unit produced different topological charges.²⁵ As shown in Figure 4d, each metalens can convert two vortex beams with different topological charges into the same diffraction-limit spot with opposite circular polarizations through spin-orbit conversion. The perovskite laser with linear polarization placed at the focal spot of the metalens is collimated into two sets of a vortex laser array on the basis of the time-reversal process, as illustrated in Figure 4e,f. Besides, they also demonstrated that perovskite based vortex micro-

lasers can achieve ultrafast all-optical switching at room temperature.⁸⁹ The donut-shaped laser beam under symmetry protection will transform into two linearly diffracted beams once the symmetry is broken. In an active system, the imaginary part of the complex refractive index can be easily steered with optical pumping, offering a flexible way to tune the symmetry. A double-pump scheme with slightly shifted spot centers is employed to investigate the switching process. As a result, ultrafast switching between a vortex beam and a linearly polarized beam is completed in 1.5 ps. Up to now, the topological charges of perovskite vortex lasers have been limited to less than 10. Dynamic control on arbitrary topological charges should draw more attention. In addition, the compactness and complexity should be considered. The emerging electrically or optically addressable dynamic metasurface^{90,91} may shed light on the compact, flexible, and dynamic control over the wavefront.

CONCLUSION AND OUTLOOK

Rapid and substantial progress has been made in perovskite lasers in the past few years. In addition to the efficient control in wavelength, mode number, emission direction, polarization, and OAM, research on the mode volume has also developed progressively. Li et al. realized nanoscale output of perovskite lasers by incorporating silver nanowires, via which the photonic modes couple into surface plasmons.⁹² Then Yu et al. reported a plasmonic nanolaser constructed by perovskite nanowires on a hybrid substrate.⁹³ The only evidence for the plasmonic mode is the transverse magnetic polarization. Huang et al. systematically investigated the comparison between photonic and plasmonic lasing mode from the viewpoint of polarization, spontaneous emission coupling factor, lifetime, and threshold and also demonstrated a plasmonic nanolaser

array.²¹ Cho et al. reported submicrometer-sized perovskite plasmonic lasers, which further reduces the mode volume in three dimensions.²³ Besides, continuous-wave pumped lasing emission from quasi-2D perovskites has been realized at room temperature,⁹⁴ laying the foundation for an electrically driven laser.

Although in rapid development, emission control in perovskite lasers is still at the early stage and much further work is needed: (1) Up to now, continuous-wave pumped ASE behavior has only been observed at low temperature,⁹⁵ which places restrictions on the future use of perovskites as gain media. More importantly, from a practical point of view, an electrically injected laser is still yet to realize. Increasing research efforts should be directed toward component regulation and passivation strategies for perovskite layers. In addition, the device configuration could draw lessons from the well-developed perovskite LEDs. Mixed-phase Ruddlesden–Popper (RP) perovskites with fast and efficient energy funneling from low-dimensional to high-dimensional quantum wells^{96,97} are potential candidates for the realization of room-temperature continuous-wave pumped ASE and an electrically driven laser. (2) Stability is a long-term issue for perovskites, which imposes an inevitable limit on the reproducibility and durability of perovskite lasers. Commonly, degradation or even decomposition occurs when perovskites are in contact with air, moisture, heat, and UV light. Encapsulation strategies by embedding perovskite into polymer matrixes,^{98,99} quartz capillary tubes,^{100,101} and dielectric nanostructures (hexagonal boron nitride flakes,¹⁰² Al₂O₃ layers,¹⁰³ silica spheres,^{104,105} or TiO₂ microtubes¹⁰⁶) have been put forward to improve the stability via isolating perovskites from air and moisture. Thermal stability and photostability can be improved by replacing the methylammonium cation with formamidinium or cesium. Additionally, RP perovskites have exhibited more stable structural and chemical properties over the three-dimensional counterparts. (3) Most of the research is restricted to the static or quasi-steady response, and yet ultrafast dynamic control over the emission wavelength, polarization and wavefront shall call more attention in the future, which is oriented to the information processing applications. In addition to the demonstrated modal interaction³⁷ and symmetry breaking⁸⁹ induced optical switching, the intrinsic carrier dynamics of perovskites should draw more attention in the ultrafast dynamic control of perovskite lasers.¹⁰⁷ (4) Electrical switching of the perovskite laser should extend from the modulation of emission intensity^{108,109} to more degrees of freedom, such as polarization, OAM, wavelength, etc. (5) Novel physics concept, e.g., parity-time symmetry breaking, should be introduced to ensure single-mode emission with selective mode order.^{110,111}

AUTHOR INFORMATION

Corresponding Authors

Shumin Xiao — Ministry of Industry and Information Technology Key Lab of Micro-Nano Optoelectronic Information System, Guangdong Provincial Key Laboratory of Semiconductor Optoelectronic Materials and Intelligent Photonic Systems, Harbin Institute of Technology, Shenzhen, Guangdong 518055, P. R. China; Collaborative Innovation Center of Extreme Optics, Shanxi University, Taiyuan, Shanxi 030006, P. R. China;  orcid.org/0000-0002-0751-9556; Email: shumin.xiao@hit.edu.cn

Qinghai Song — Ministry of Industry and Information Technology Key Lab of Micro-Nano Optoelectronic Information System, Guangdong Provincial Key Laboratory of Semiconductor Optoelectronic Materials and Intelligent Photonic Systems, Harbin Institute of Technology, Shenzhen, Guangdong 518055, P. R. China; Collaborative Innovation Center of Extreme Optics, Shanxi University, Taiyuan, Shanxi 030006, P. R. China;  orcid.org/0000-0003-1048-411X; Email: qinghai.song@hit.edu.cn

Authors

Kaiyang Wang — Ministry of Industry and Information Technology Key Lab of Micro-Nano Optoelectronic Information System, Guangdong Provincial Key Laboratory of Semiconductor Optoelectronic Materials and Intelligent Photonic Systems, Harbin Institute of Technology, Shenzhen, Guangdong 518055, P. R. China; Collaborative Innovation Center of Extreme Optics, Shanxi University, Taiyuan, Shanxi 030006, P. R. China;  orcid.org/0000-0001-6052-6408

Can Huang — Ministry of Industry and Information Technology Key Lab of Micro-Nano Optoelectronic Information System, Guangdong Provincial Key Laboratory of Semiconductor Optoelectronic Materials and Intelligent Photonic Systems, Harbin Institute of Technology, Shenzhen, Guangdong 518055, P. R. China; Collaborative Innovation Center of Extreme Optics, Shanxi University, Taiyuan, Shanxi 030006, P. R. China

Qifeng Ruan — Ministry of Industry and Information Technology Key Lab of Micro-Nano Optoelectronic Information System, Guangdong Provincial Key Laboratory of Semiconductor Optoelectronic Materials and Intelligent Photonic Systems, Harbin Institute of Technology, Shenzhen, Guangdong 518055, P. R. China; Collaborative Innovation Center of Extreme Optics, Shanxi University, Taiyuan, Shanxi 030006, P. R. China;  orcid.org/0000-0002-1592-9010

Yu Zhou — Ministry of Industry and Information Technology Key Lab of Micro-Nano Optoelectronic Information System, Guangdong Provincial Key Laboratory of Semiconductor Optoelectronic Materials and Intelligent Photonic Systems, Harbin Institute of Technology, Shenzhen, Guangdong 518055, P. R. China; Collaborative Innovation Center of Extreme Optics, Shanxi University, Taiyuan, Shanxi 030006, P. R. China

Yimu Chen — Ministry of Industry and Information Technology Key Lab of Micro-Nano Optoelectronic Information System, Guangdong Provincial Key Laboratory of Semiconductor Optoelectronic Materials and Intelligent Photonic Systems, Harbin Institute of Technology, Shenzhen, Guangdong 518055, P. R. China; Collaborative Innovation Center of Extreme Optics, Shanxi University, Taiyuan, Shanxi 030006, P. R. China

Haoliang Liu — Ministry of Industry and Information Technology Key Lab of Micro-Nano Optoelectronic Information System, Guangdong Provincial Key Laboratory of Semiconductor Optoelectronic Materials and Intelligent Photonic Systems, Harbin Institute of Technology, Shenzhen, Guangdong 518055, P. R. China; Collaborative Innovation Center of Extreme Optics, Shanxi University, Taiyuan, Shanxi 030006, P. R. China

Complete contact information is available at:

<https://pubs.acs.org/10.1021/acspophotonics.2c01658>

Author Contributions

[†]K.W. and C.H. contributed equally.

Notes

The authors declare no competing financial interest.

ACKNOWLEDGMENTS

We acknowledge financial support from National Key Research and Development Program of China (Grant Nos. 2021YFA1400802, 2018YFB2200403), National Natural Science Foundation of China (Grant Nos. 11974092, 12025402, 61975041, 91850204, 11934012, 12204133, 12261131500), Fundamental Research Funds for the Central Universities (2022FRRK030004, HIT.BRET.2021009), and Shenzhen Fundamental Research Projects (Grant Nos. JCYJ20200109112805990, JCYJ20220818102218040, JCYJ20200109113003946, JCYJ20210324120402006, JCYJ20180507183532343, JCYJ20180507184613841, GXWD20220817145518001).

REFERENCES

- (1) Best Research-Cell Efficiencies. <https://www.nrel.gov/pv/cell-efficiency.html> (accessed: June 2022).
- (2) Kojima, A.; Teshima, K.; Shirai, Y.; Miyasaka, T. Organometal halide perovskites as visible-light sensitizers for photovoltaic cells. *J. Am. Chem. Soc.* **2009**, *131* (17), 6050–6051.
- (3) Ma, D.; Lin, K.; Dong, Y.; Chouiba, H.; Proppe, A. H.; Wu, D.; Wang, Y. K.; Chen, B.; Li, P.; Fan, J. Z.; Yuan, F.; Johnston, A.; Liu, Y.; Kang, Y.; Lu, Z. H.; Wei, Z.; Sargent, E. H. Distribution control enables efficient reduced-dimensional perovskite LEDs. *Nature* **2021**, *599* (7886), 594–598.
- (4) Xiang, H.; Wang, R.; Chen, J.; Li, F.; Zeng, H. Research progress of full electroluminescent white light-emitting diodes based on a single emissive layer. *Light: Sci. Appl.* **2021**, *10* (1), 206.
- (5) Zhang, L.; Sun, C.; He, T.; Jiang, Y.; Wei, J.; Huang, Y.; Yuan, M. High-performance quasi-2D perovskite light-emitting diodes: from materials to devices. *Light: Sci. Appl.* **2021**, *10* (1), 61.
- (6) Kim, W.; Kim, H.; Yoo, T. J.; Lee, J. Y.; Jo, J. Y.; Lee, B. H.; Sasikala, A. A.; Jung, G. Y.; Pak, Y. Perovskite multifunctional logic gates via bipolar photoresponse of single photodetector. *Nat. Commun.* **2022**, *13* (1), 720.
- (7) Feng, X.; He, Y.; Qu, W.; Song, J.; Pan, W.; Tan, M.; Yang, B.; Wei, H. Spray-coated perovskite hemispherical photodetector featuring narrow-band and wide-angle imaging. *Nat. Commun.* **2022**, *13* (1), 6106.
- (8) Wang, F.; Zou, X.; Xu, M.; Wang, H.; Wang, H.; Guo, H.; Guo, J.; Wang, P.; Peng, M.; Wang, Z.; Wang, Y.; Miao, J.; Chen, F.; Wang, J.; Chen, X.; Pan, A.; Shan, C.; Liao, L.; Hu, W. Recent Progress on Electrical and Optical Manipulations of Perovskite Photodetectors. *Adv. Sci.* **2021**, *8*, 2100569.
- (9) Pang, J.; Zhao, S.; Du, X.; Wu, H.; Niu, G.; Tang, J. Vertical matrix perovskite X-ray detector for effective multi-energy discrimination. *Light: Sci. Appl.* **2022**, *11* (1), 105.
- (10) Zhou, Y.; Zhao, L.; Ni, Z.; Xu, S.; Zhao, J.; Xiao, X.; Huang, J. Heterojunction structures for reduced noise in large-area and sensitive perovskite x-ray detectors. *Sci. Adv.* **2021**, *7* (36), eabg6716.
- (11) Peng, J.; Xia, C. Q.; Xu, Y.; Li, R.; Cui, L.; Clegg, J. K.; Herz, L. M.; Johnston, M. B.; Lin, Q. Crystallization of CsPbBr₃ single crystals in water for X-ray detection. *Nat. Commun.* **2021**, *12* (1), 1531.
- (12) Sutherland, B. R.; Sargent, E. H. Perovskite photonic sources. *Nat. Photonics* **2016**, *10* (5), 295–302.
- (13) Zhang, Q.; Su, R.; Du, W.; Liu, X.; Zhao, L.; Ha, S. T.; Xiong, Q. Advances in Small Perovskite-Based Lasers. *Small Methods* **2017**, *1* (9), 1700163.
- (14) Wang, K.; Wang, S.; Xiao, S.; Song, Q. Recent Advances in Perovskite Micro- and Nanolasers. *Adv. Opt. Mater.* **2018**, *6* (18), 1800278.
- (15) Xing, G.; Mathews, N.; Lim, S. S.; Yantara, N.; Liu, X.; Sabba, D.; Gratzel, M.; Mhaisalkar, S.; Sum, T. C. Low-temperature solution-processed wavelength-tunable perovskites for lasing. *Nat. Mater.* **2014**, *13* (5), 476–80.
- (16) Zhu, H.; Fu, Y.; Meng, F.; Wu, X.; Gong, Z.; Ding, Q.; Gustafsson, M. V.; Trinh, M. T.; Jin, S.; Zhu, X. Y. Lead halide perovskite nanowire lasers with low lasing thresholds and high quality factors. *Nat. Mater.* **2015**, *14* (6), 636–42.
- (17) Wang, K.; Sun, S.; Zhang, C.; Sun, W.; Gu, Z.; Xiao, S.; Song, Q. Whispering-gallery-mode based CH₃NH₃PbBr₃ perovskite micro-rod lasers with high quality factors. *Mater. Chem. Front.* **2017**, *1* (3), 477–481.
- (18) Zhang, N.; Sun, W.; Rodrigues, S. P.; Wang, K.; Gu, Z.; Wang, S.; Cai, W.; Xiao, S.; Song, Q. Highly Reproducible Organometallic Halide Perovskite Microdevices based on Top-Down Lithography. *Adv. Mater.* **2017**, *29* (15), 1606205.
- (19) Tang, B.; Sun, L.; Zheng, W.; Dong, H.; Zhao, B.; Si, Q.; Wang, X.; Jiang, X.; Pan, A.; Zhang, L. Ultrahigh Quality Upconverted Single-Mode Lasing in Cesium Lead Bromide Spherical Microcavity. *Adv. Opt. Mater.* **2018**, *6* (20), 1800391.
- (20) Wang, K.; Sun, W.; Li, J.; Gu, Z.; Xiao, S.; Song, Q. Unidirectional Lasing Emissions from CH₃NH₃PbBr₃ Perovskite Microdisks. *ACS Photonics* **2016**, *3* (6), 1125–1130.
- (21) Huang, C.; Sun, W.; Fan, Y.; Wang, Y.; Gao, Y.; Zhang, N.; Wang, K.; Liu, S.; Wang, S.; Xiao, S.; Song, Q. Formation of Lead Halide Perovskite Based Plasmonic Nanolasers and Nanolaser Arrays by Tailoring the Substrate. *ACS Nano* **2018**, *12* (4), 3865–3874.
- (22) Wu, Z.; Chen, J.; Mi, Y.; Sui, X.; Zhang, S.; Du, W.; Wang, R.; Shi, J.; Wu, X.; Qiu, X.; Qin, Z.; Zhang, Q.; Liu, X. All-Inorganic CsPbBr₃ Nanowire Based Plasmonic Lasers. *Adv. Opt. Mater.* **2018**, *6* (22), 1800674.
- (23) Cho, S.; Yang, Y.; Soljacic, M.; Yun, S. H. Submicrometer perovskite plasmonic lasers at room temperature. *Sci. Adv.* **2021**, *7* (35), eabf3362.
- (24) Sun, W.; Liu, Y.; Qu, G.; Fan, Y.; Dai, W.; Wang, Y.; Song, Q.; Han, J.; Xiao, S. Lead halide perovskite vortex microlasers. *Nat. Commun.* **2020**, *11* (1), 4862.
- (25) Zhang, H.; Sha, X.; Chen, Q.; Cheng, J.; Ji, Z.; Song, Q.; Yu, S.; Xiao, S. All-Dielectric Metasurface-Enabled Multiple Vortex Emissions. *Adv. Mater.* **2022**, *34* (14), 2109255.
- (26) Dai, W.; Wang, Y.; Li, R.; Fan, Y.; Qu, G.; Wu, Y.; Song, Q.; Han, J.; Xiao, S. Achieving Circularly Polarized Surface Emitting Perovskite Microlasers with All-Dielectric Metasurfaces. *ACS Nano* **2020**, *14* (12), 17063–17070.
- (27) Xing, G.; Kumar, M. H.; Chong, W. K.; Liu, X.; Cai, Y.; Ding, H.; Asta, M.; Gratzel, M.; Mhaisalkar, S.; Mathews, N.; Sum, T. C. Solution-Processed Tin-Based Perovskite for Near-Infrared Lasing. *Adv. Mater.* **2016**, *28* (37), 8191–8196.
- (28) Fu, Y. Stabilization of Metastable Halide Perovskite Lattices in the 2D Limit. *Adv. Mater.* **2022**, *34*, 2108556.
- (29) Pan, D.; Fu, Y.; Chen, J.; Czech, K. J.; Wright, J. C.; Jin, S. Visualization and Studies of Ion-Diffusion Kinetics in Cesium Lead Bromide Perovskite Nanowires. *Nano Lett.* **2018**, *18* (3), 1807–1813.
- (30) Akkerman, Q. A.; D’Innocenzo, V.; Accornero, S.; Scarpellini, A.; Petrozza, A.; Prato, M.; Manna, L. Tuning the Optical Properties of Cesium Lead Halide Perovskite Nanocrystals by Anion Exchange Reactions. *J. Am. Chem. Soc.* **2015**, *137* (32), 10276–81.
- (31) Li, G.; Ho, J. Y.-L.; Wong, M.; Kwok, H. S. Reversible Anion Exchange Reaction in Solid Halide Perovskites and Its Implication in Photovoltaics. *J. Phys. Chem. C* **2015**, *119* (48), 26883–26888.
- (32) Wong, A. B.; Lai, M.; Eaton, S. W.; Yu, Y.; Lin, E.; Dou, L.; Fu, A.; Yang, P. Growth and Anion Exchange Conversion of CH₃NH₃PbX₃ Nanorod Arrays for Light-Emitting Diodes. *Nano Lett.* **2015**, *15* (8), 5519–24.
- (33) Zhang, N.; Wang, K.; Wei, H.; Gu, Z.; Sun, W.; Li, J.; Xiao, S.; Song, Q. Postsynthetic and Selective Control of Lead Halide Perovskite Microlasers. *J. Phys. Chem. Lett.* **2016**, *7* (19), 3886–3891.
- (34) Xing, J.; Liu, X. F.; Zhang, Q.; Ha, S. T.; Yuan, Y. W.; Shen, C.; Sum, T. C.; Xiong, Q. Vapor Phase Synthesis of Organometal Halide

- Perovskite Nanowires for Tunable Room-Temperature Nanolasers. *Nano Lett.* **2015**, *15* (7), 4571–4577.
- (35) Yang, Z.; Lu, J.; ZhuGe, M.; Cheng, Y.; Hu, J.; Li, F.; Qiao, S.; Zhang, Y.; Hu, G.; Yang, Q.; Peng, D.; Liu, K.; Pan, C. Controllable Growth of Aligned Monocrystalline CsPbBr₃Microwire Arrays for Piezoelectric-Induced Dynamic Modulation of Single-Mode Lasing. *Adv. Mater.* **2019**, *31* (18), 1900647.
- (36) Chen, L. J.; Dai, J. H.; Lin, J. D.; Mo, T. S.; Lin, H. P.; Yeh, H. C.; Chuang, Y. C.; Jiang, S. A.; Lee, C. R. Wavelength-Tunable and Highly Stable Perovskite-Quantum-Dot-Doped Lasers with Liquid Crystal Lasing Cavities. *ACS Appl. Mater. Interfaces* **2018**, *10* (39), 33307–33315.
- (37) Zhang, N.; Fan, Y.; Wang, K.; Gu, Z.; Wang, Y.; Ge, L.; Xiao, S.; Song, Q. All-optical control of lead halide perovskite microlasers. *Nat. Commun.* **2019**, *10* (1), 1770.
- (38) Ge, L.; Liu, D.; Cerjan, A.; Rotter, S.; Cao, H.; Johnson, S. G.; Türeci, H. E.; Stone, A. D. Interaction-induced mode switching in steady-state microlasers. *Opt. Express* **2016**, *24* (1), 41–54.
- (39) Tang, B.; Hu, Y.; Lu, J.; Dong, H.; Mou, N.; Gao, X.; Wang, H.; Jiang, X.; Zhang, L. Energy transfer and wavelength tunable lasing of single perovskite alloy nanowire. *Nano Energy* **2020**, *71*, 104641.
- (40) Zhao, J.; Yan, Y.; Wei, C.; Zhang, W.; Gao, Z.; Zhao, Y. S. Switchable Single-Mode Perovskite Microlasers Modulated by Responsive Organic Microdisks. *Nano Lett.* **2018**, *18* (2), 1241–1245.
- (41) Chen, S.; Zhang, C.; Lee, J.; Han, J.; Nurmiikko, A. High-Q Low-Threshold Monolithic Perovskite Thin-Film Vertical-Cavity Lasers. *Adv. Mater.* **2017**, *29* (16), 1604781.
- (42) Chen, S. T.; Nurmiikko, A. Stable Green Perovskite Vertical-Cavity Surface-Emitting Lasers on Rigid and Flexible Substrates. *ACS Photonics* **2017**, *4* (10), 2486–2494.
- (43) Pourdavoud, N.; Wang, S.; Mayer, A.; Hu, T.; Chen, Y.; Marianovich, A.; Kowalsky, W.; Heiderhoff, R.; Scheer, H. C.; Riedl, T. Photonic Nanostructures Patterned by Thermal Nanoimprint Directly into Organo-Metal Halide Perovskites. *Adv. Mater.* **2017**, *29* (12), 1605003.
- (44) Cha, H.; Bae, S.; Lee, M.; Jeon, H. Two-dimensional photonic crystal bandedge laser with hybrid perovskite thin film for optical gain. *Appl. Phys. Lett.* **2016**, *108* (18), 181104.
- (45) Chen, S.; Roh, K.; Lee, J.; Chong, W. K.; Lu, Y.; Mathews, N.; Sum, T. C.; Nurmiikko, A. A Photonic Crystal Laser from Solution Based Organo-Lead Iodide Perovskite Thin Films. *ACS Nano* **2016**, *10* (4), 3959–3967.
- (46) Jia, Y.; Kerner, R. A.; Grede, A. J.; Brigeman, A. N.; Rand, B. P.; Giebink, N. C. Diode-Pumped Organo-Lead Halide Perovskite Lasing in a Metal-Clad Distributed Feedback Resonator. *Nano Lett.* **2016**, *16* (7), 4624–4629.
- (47) Saliba, M.; Wood, S. M.; Patel, J. B.; Nayak, P. K.; Huang, J.; Alexander-Webber, J. A.; Wenger, B.; Stranks, S. D.; Horantner, M. T.; Wang, J. T.; Nicholas, R. J.; Herz, L. M.; Johnston, M. B.; Morris, S. M.; Snaith, H. J.; Riede, M. K. Structured Organic-Inorganic Perovskite toward a Distributed Feedback Laser. *Adv. Mater.* **2016**, *28* (5), 923–929.
- (48) Bar-On, O.; Brenner, P.; Lemmer, U.; Scheuer, J. Micro Lasers by Scalable Lithography of Metal-Halide Perovskites. *Adv. Mater. Technol.* **2018**, *3* (12), 1800212.
- (49) Huang, C.-Y.; Zou, C.; Mao, C.; Corp, K. L.; Yao, Y.-C.; Lee, Y.-J.; Schlenker, C. W.; Jen, A. K. Y.; Lin, L. Y. CsPbBr₃ Perovskite Quantum Dot Vertical Cavity Lasers with Low Threshold and High Stability. *ACS Photonics* **2017**, *4* (9), 2281–2289.
- (50) Wang, Y.; Li, X.; Nalla, V.; Zeng, H.; Sun, H. Solution-Processed Low Threshold Vertical Cavity Surface Emitting Lasers from All-Inorganic Perovskite Nanocrystals. *Adv. Funct. Mater.* **2017**, *27*, 1605088.
- (51) Liao, Q.; Hu, K.; Zhang, H.; Wang, X.; Yao, J.; Fu, H. Perovskite Microdisk Microlasers Self-Assembled from Solution. *Adv. Mater.* **2015**, *27* (22), 3405–3410.
- (52) Tang, B.; Dong, H.; Sun, L.; Zheng, W.; Wang, Q.; Sun, F.; Jiang, X.; Pan, A.; Zhang, L. Single-Mode Lasers Based on Cesium Lead Halide Perovskite Submicron Spheres. *ACS Nano* **2017**, *11* (11), 10681–10688.
- (53) Wang, K.; Gu, Z.; Liu, S.; Li, J.; Xiao, S.; Song, Q. Formation of single-mode laser in transverse plane of perovskite microwire via micromanipulation. *Opt. Lett.* **2016**, *41* (3), 555–558.
- (54) Wang, K.; Sun, W.; Wang, S.; Liu, S.; Zhang, N.; Xiao, S.; Song, Q. Single Crystal Microrod Based Homonuclear Photonic Molecule Lasers. *Adv. Opt. Mater.* **2017**, *5* (3), 1600744.
- (55) Wang, K.; Gu, Z.; Liu, S.; Sun, W.; Zhang, N.; Xiao, S.; Song, Q. High-Density and Uniform Lead Halide Perovskite Nanolaser Array on Silicon. *J. Phys. Chem. Lett.* **2016**, *7* (13), 2549–2555.
- (56) Boeck, R.; Jaeger, N. A.; Rouger, N.; Chrostowski, L. Series-coupled silicon racetrack resonators and the Vernier effect: theory and measurement. *Opt. Express* **2010**, *18* (24), 25151–25157.
- (57) Claes, T.; Bogaerts, W.; Bienstman, P. Experimental characterization of a silicon photonic biosensor consisting of two cascaded ring resonators based on the Vernier-effect and introduction of a curve fitting method for an improved detection limit. *Opt. Express* **2010**, *18* (22), 22747–22761.
- (58) Hulme, J. C.; Doylend, J. K.; Bowers, J. E. Widely tunable Vernier ring laser on hybrid silicon. *Opt. Express* **2013**, *21* (17), 19718–19722.
- (59) Ge, L.; Türeci, H. E. Inverse Vernier effect in coupled lasers. *Phys. Rev. A* **2015**, *92* (1), No. 013840.
- (60) Li, M.; Zhang, N.; Wang, K.; Li, J.; Xiao, S.; Song, Q. Inversed Vernier effect based single-mode laser emission in coupled microdisks. *Sci. Rep.* **2015**, *5*, 13682.
- (61) Gomes, A. D.; Bartelt, H.; Frazão, O. Optical Vernier Effect: Recent Advances and Developments. *Laser Photonics Rev.* **2021**, *15* (7), 2000588.
- (62) Li, F.; Jiang, M.; Cheng, Y.; Zhang, Y.; Yang, Z.; Peng, Y.; Ma, W.; Chen, Q.; Wang, C.; Liu, K.; Wang, R.; Lu, J.; Pan, C. Single-mode lasing of CsPbBr₃ perovskite NWs enabled by the Vernier effect. *Nanoscale* **2021**, *13* (8), 4432–4438.
- (63) Zhou, B. E.; Jiang, M. M.; Dong, H. X.; Zheng, W. H.; Huang, Y. Z.; Han, J. Y.; Pan, A. L.; Zhang, L. High-Temperature Upconverted Single-Mode Lasing in 3D Fully Inorganic Perovskite Microcubic Cavity. *ACS Photonics* **2019**, *6* (3), 793–801.
- (64) Tiguntseva, E.; Koshelev, K.; Furasova, A.; Tonkaev, P.; Mikhailovskii, V.; Ushakova, E. V.; Baranov, D. G.; Shegai, T.; Zakhidov, A. A.; Kivshar, Y.; Makarov, S. V. Room-Temperature Lasing from Mie-Resonant Nonplasmonic Nanoparticles. *ACS Nano* **2020**, *14* (7), 8149–8156.
- (65) Liu, X.; Niu, L.; Wu, C.; Cong, C.; Wang, H.; Zeng, Q.; He, H.; Fu, Q.; Fu, W.; Yu, T.; Jin, C.; Liu, Z.; Sum, T. C. Periodic Organic-Inorganic Halide Perovskite Microplatelet Arrays on Silicon Substrates for Room-Temperature Lasing. *Adv. Sci.* **2016**, *3* (11), 1600137.
- (66) He, X.; Liu, P.; Zhang, H.; Liao, Q.; Yao, J.; Fu, H. Patterning Multicolored Microdisk Laser Arrays of Cesium Lead Halide Perovskite. *Adv. Mater.* **2017**, *29* (12), 1604510.
- (67) Pourdavoud, N.; Haeger, T.; Mayer, A.; Cegielski, P. J.; Giesecke, A. L.; Heiderhoff, R.; Olthof, S.; Zaeffferer, S.; Shutsko, I.; Henkel, A.; Becker-Koch, D.; Stein, M.; Cehovski, M.; Charfi, O.; Johannes, H. H.; Rogalla, D.; Lemme, M. C.; Koch, M.; Vaynzof, Y.; Meerholz, K.; Kowalsky, W.; Scheer, H. C.; Gorrn, P.; Riedl, T. Room-Temperature Stimulated Emission and Lasing in Recrystallized Cesium Lead Bromide Perovskite Thin Films. *Adv. Mater.* **2019**, e1903717.
- (68) Zhizhchenko, A.; Syubaev, S.; Berestennikov, A.; Yulin, A. V.; Porfirev, A.; Pushkarev, A.; Shishkin, I.; Golokhvast, K.; Bogdanov, A. A.; Zakhidov, A. A.; Kuchmizhak, A. A.; Kivshar, Y. S.; Makarov, S. V. Single-Mode Lasing from Imprinted Halide-Perovskite Microdisks. *ACS Nano* **2019**, *13* (4), 4140–4147.
- (69) Zhong, Y.; Liao, K.; Du, W.; Zhu, J.; Shang, Q.; Zhou, F.; Wu, X.; Sui, X.; Shi, J.; Yue, S.; Wang, Q.; Zhang, Y.; Zhang, Q.; Hu, X.; Liu, X. Large-Scale Thin CsPbBr₃ Single-Crystal Film Grown on Sapphire via Chemical Vapor Deposition: Toward Laser Array Application. *ACS Nano* **2020**, *14* (11), 15605–15615.

- (70) Cao, H.; Chiriki, R.; Bittner, S.; Friesem, A. A.; Davidson, N. Complex lasers with controllable coherence. *Nat. Rev. Phys.* **2019**, *1* (2), 156–168.
- (71) Liu, Y.; Yang, W.; Xiao, S.; Zhang, N.; Fan, Y.; Qu, G.; Song, Q. Surface-Emitting Perovskite Random Lasers for Speckle-Free Imaging. *ACS Nano* **2019**, *13* (9), 10653–10661.
- (72) Zhizhchenko, A. Y.; Cherepakhin, A. B.; Masharin, M. A.; Pushkarev, A. P.; Kulinich, S. A.; Kuchmizhak, A. A.; Makarov, S. V. Directional Lasing from Nanopatterned Halide Perovskite Nanowire. *Nano Lett.* **2021**, *21* (23), 10019–10025.
- (73) Trofimov, P.; Pushkarev, A. P.; Sinev, I. S.; Fedorov, V. V.; Bruyere, S.; Bolshakov, A.; Mukhin, I. S.; Makarov, S. V. Perovskite-Gallium Phosphide Platform for Reconfigurable Visible-Light Nanophotonic Chip. *ACS Nano* **2020**, *14* (7), 8126–8134.
- (74) Gu, Z. Y.; Sun, W. Z.; Wang, K. Y.; Zhang, N.; Zhang, C.; Lyu, Q.; Li, J. K.; Xiao, S. M.; Song, Q. H. Hybridizing CH₃NH₃PbBr₃ microwires and tapered Fibers for efficient light collection. *J. Mater. Chem. A* **2016**, *4* (21), 8015–8019.
- (75) Cegielski, P. J.; Neutzner, S.; Porschatis, C.; Lerch, H.; Bolten, J.; Suckow, S.; Kandada, A. R. S.; Chmielak, B.; Petrozza, A.; Wahlbrink, T.; Giesecke, A. L. Integrated perovskite lasers on a silicon nitride waveguide platform by cost-effective high throughput fabrication. *Opt. Express* **2017**, *25* (12), 13199–13206.
- (76) Cegielski, P. J.; Giesecke, A. L.; Neutzner, S.; Porschatis, C.; Gandini, M.; Schall, D.; Perini, C. A. R.; Bolten, J.; Suckow, S.; Kataria, S.; Chmielak, B.; Wahlbrink, T.; Petrozza, A.; Lemme, M. C. Monolithically Integrated Perovskite Semiconductor Lasers on Silicon Photonic Chips by Scalable Top-Down Fabrication. *Nano Lett.* **2018**, *18* (11), 6915–6923.
- (77) Wu, X.; Li, H.; Liu, L.; Xu, L. Unidirectional single-frequency lasing from a ring-spiral coupled microcavity laser. *Appl. Phys. Lett.* **2008**, *93* (8), No. 081105.
- (78) Wang, S.; Liu, Y. L.; Li, G.; Zhang, J.; Zhang, N.; Xiao, S. M.; Song, Q. H. Lead Halide Perovskite Based Microdisk Lasers for On-Chip Integrated Photonic Circuits. *Adv. Opt. Mater.* **2018**, *6* (6), 1701266.
- (79) Brenner, P.; Stulz, M.; Kapp, D.; Abzieher, T.; Paetzold, U. W.; Quintilla, A.; Howard, I. A.; Kalt, H.; Lemmer, U. Highly stable solution processed metal-halide perovskite lasers on nanoimprinted distributed feedback structures. *Appl. Phys. Lett.* **2016**, *109* (14), 141106.
- (80) Duan, Z.; Wang, Y.; Li, G.; Wang, S.; Yi, N.; Liu, S.; Xiao, S.; Song, Q. Chip-Scale Fabrication of Uniform Lead Halide Perovskites Microlaser Array and Photodetector Array. *Laser Photonics Rev.* **2018**, *12* (1), 1700234.
- (81) Gao, Y.; Zhao, L.; Shang, Q.; Zhong, Y.; Liu, Z.; Chen, J.; Zhang, Z.; Shi, J.; Du, W.; Zhang, Y.; Chen, S.; Gao, P.; Liu, X.; Wang, X.; Zhang, Q. Ultrathin CsPbX₃ Nanowire Arrays with Strong Emission Anisotropy. *Adv. Mater.* **2018**, *30* (31), 1801805.
- (82) Du, W.; Wu, X.; Zhang, S.; Sui, X.; Jiang, C.; Zhu, Z.; Shang, Q.; Shi, J.; Yue, S.; Zhang, Q.; Zhang, J.; Liu, X. All Optical Switching through Anisotropic Gain of CsPbBr₃ Single Crystal Microplatelet. *Nano Lett.* **2022**, *22* (10), 4049–4057.
- (83) Seo, I. C.; Lim, Y.; An, S. C.; Woo, B. H.; Kim, S.; Son, J. G.; Yoo, S.; Park, Q. H.; Kim, J. Y.; Jun, Y. C. Circularly Polarized Emission from Organic-Inorganic Hybrid Perovskites via Chiral Fano Resonances. *ACS Nano* **2021**, *15* (8), 13781–13793.
- (84) Lim, Y.; Seo, I. C.; An, S. C.; Kim, Y.; Park, C.; Woo, B. H.; Kim, S.; Park, H. R.; Jun, Y. C. Maximally Chiral Emission via Chiral Quasibound States in the Continuum. *Laser Photonics Rev.* **2023**, *17*, 2200611.
- (85) Long, G.; Adamo, G.; Tian, J.; Klein, M.; Krishnamoorthy, H. N. S.; Feltri, E.; Wang, H.; Soci, C. Perovskite metasurfaces with large superstructural chirality. *Nat. Commun.* **2022**, *13* (1), 1551.
- (86) Zhang, X.; Liu, Y.; Han, J.; Kivshar, Y.; Song, Q. Chiral emission from resonant metasurfaces. *Science* **2022**, *377* (6611), 1215–1218.
- (87) Yao, A. M.; Padgett, M. J. Orbital angular momentum: origins, behavior and applications. *Adv. Opt. Photonics* **2011**, *3* (2), 161.
- (88) Shen, Y.; Wang, X.; Xie, Z.; Min, C.; Fu, X.; Liu, Q.; Gong, M.; Yuan, X. Optical vortices 30 years on: OAM manipulation from topological charge to multiple singularities. *Light: Sci. Appl.* **2019**, *8*, 90.
- (89) Huang, C.; Zhang, C.; Xiao, S.; Wang, Y.; Fan, Y.; Liu, Y.; Zhang, N.; Qu, G.; Ji, H.; Han, J.; Ge, L.; Kivshar, Y.; Song, Q. Ultrafast control of vortex microlasers. *Science* **2020**, *367* (6481), 1018–1021.
- (90) Wuttig, M.; Bhaskaran, H.; Taubner, T. Phase-change materials for non-volatile photonic applications. *Nat. Photonics* **2017**, *11* (8), 465–476.
- (91) Zhang, Y.; Fowler, C.; Liang, J.; Azhar, B.; Shalaginov, M. Y.; Deckoff-Jones, S.; An, S.; Chou, J. B.; Roberts, C. M.; Liberman, V.; Kang, M.; Rios, C.; Richardson, K. A.; Rivero-Baleine, C.; Gu, T.; Zhang, H.; Hu, J. Electrically reconfigurable non-volatile metasurface using low-loss optical phase-change material. *Nat. Nanotechnol.* **2021**, *16* (6), 661–666.
- (92) Li, Y. J.; Lv, Y.; Zou, C. L.; Zhang, W.; Yao, J.; Zhao, Y. S. Output Coupling of Perovskite Lasers from Embedded Nanoscale Plasmonic Waveguides. *J. Am. Chem. Soc.* **2016**, *138* (7), 2122–2125.
- (93) Yu, H.; Ren, K.; Wu, Q.; Wang, J.; Lin, J.; Wang, Z.; Xu, J.; Oulton, R. F.; Qu, S.; Jin, P. Organic-inorganic perovskite plasmonic nanowire lasers with a low threshold and a good thermal stability. *Nanoscale* **2016**, *8* (47), 19536–19540.
- (94) Qin, C.; Sandanayaka, A. S. D.; Zhao, C.; Matsushima, T.; Zhang, D.; Fujihara, T.; Adachi, C. Stable room-temperature continuous-wave lasing in quasi-2D perovskite films. *Nature* **2020**, *585* (7823), 53–57.
- (95) Brenner, P.; Bar-On, O.; Jakoby, M.; Allegro, I.; Richards, B. S.; Paetzold, U. W.; Howard, I. A.; Scheuer, J.; Lemmer, U. Continuous wave amplified spontaneous emission in phase-stable lead halide perovskites. *Nat. Commun.* **2019**, *10* (1), 988.
- (96) Xing, G.; Wu, B.; Wu, X.; Li, M.; Du, B.; Wei, Q.; Guo, J.; Yeow, E. K.; Sum, T. C.; Huang, W. Transcending the slow bimolecular recombination in lead-halide perovskites for electroluminescence. *Nat. Commun.* **2017**, *8*, 14558.
- (97) Guo, J.; Liu, T.; Li, M.; Liang, C.; Wang, K.; Hong, G.; Tang, Y.; Long, G.; Yu, S. F.; Lee, T. W.; Huang, W.; Xing, G. Ultrashort laser pulse doubling by metal-halide perovskite multiple quantum wells. *Nat. Commun.* **2020**, *11* (1), 3361.
- (98) Suarez, I.; Juarez-Perez, E. J.; Bisquert, J.; Mora-Sero, I.; Martinez-Pastor, J. P. Polymer/Perovskite Amplifying Waveguides for Active Hybrid Silicon Photonics. *Adv. Mater.* **2015**, *27* (40), 6157–6162.
- (99) Zhang, H.; Liao, Q.; Wang, X.; Yao, J.; Fu, H. Water-Resistant Perovskite Polygonal Microdisks Laser in Flexible Photonics Devices. *Adv. Opt. Mater.* **2016**, *4* (11), 1718–1725.
- (100) Kurahashi, N.; Nguyen, V.-C.; Sasaki, F.; Yanagi, H. Whispering gallery mode lasing in lead halide perovskite crystals grown in microcapillary. *Appl. Phys. Lett.* **2018**, *113* (1), No. 011107.
- (101) Liu, Z. Z.; Hu, Z. P.; Zhang, Z. Y.; Du, J.; Yang, J.; Tang, X. S.; Liu, W. M.; Leng, Y. X. Two-Photon Pumped Amplified Spontaneous Emission and Lasing from Formamidinium Lead Bromine Nanocrystals. *ACS Photonics* **2019**, *6* (12), 3150–3158.
- (102) Yu, H.; Cheng, X.; Wang, Y.; Liu, Y.; Rong, K.; Li, Z.; Wan, Y.; Gong, W.; Watanabe, K.; Taniguchi, T.; Wang, S.; Chen, J.; Ye, Y.; Dai, L. Waterproof Perovskite-Hexagonal Boron Nitride Hybrid Nanolasers with Low Lasing Thresholds and High Operating Temperature. *ACS Photonics* **2018**, *5* (11), 4520–4528.
- (103) Yu, H.; Xu, X.; Liu, H.; Wan, Y.; Cheng, X.; Chen, J.; Ye, Y.; Dai, L. Waterproof Cesium Lead Bromide Perovskite Lasers and Their Applications in Solution. *ACS Nano* **2020**, *14* (1), 552–558.
- (104) Liu, Z.; Hu, Z.; Shi, T.; Du, J.; Yang, J.; Zhang, Z.; Tang, X.; Leng, Y. Stable and enhanced frequency up-converted lasing from CsPbBr₃ quantum dots embedded in silica sphere. *Opt. Express* **2019**, *27* (7), 9459–9466.
- (105) Li, S.; Lei, D.; Ren, W.; Guo, X.; Wu, S.; Zhu, Y.; Rogach, A. L.; Chhowalla, M.; Jen, A. K. Water-resistant perovskite nanodots

- enable robust two-photon lasing in aqueous environment. *Nat. Commun.* **2020**, *11* (1), 1192.
- (106) Tang, X.; Bian, Y.; Liu, Z.; Du, J.; Li, M.; Hu, Z.; Yang, J.; Chen, W.; Sun, L. Room-temperature up-conversion random lasing from CsPbBr₃ quantum dots with TiO₂ nanotubes. *Opt. Lett.* **2019**, *44* (19), 4706–4709.
- (107) Zhang, X.; Wang, M.; Ma, L.; Fu, Y.; Guo, J.; Ma, H.; Zhang, Y.; Yan, Z.; Han, X. Ultrafast two-photon optical switch using single crystal hybrid halide perovskites. *Optica* **2021**, *8* (5), 735.
- (108) Gao, Y.; Li, X.; Liu, W.; Xing, X.; Long, H.; Wang, K.; Wang, B.; Lu, P. Highly Tunable Enhancement and Switching of Nonlinear Emission from All-Inorganic Lead Halide Perovskites via Electric Field. *Nano Lett.* **2021**, *21* (24), 10230–10237.
- (109) Qin, Z.; Zhang, C.; Chen, L.; Yu, T.; Wang, X.; Xiao, M. Electrical Switching of Optical Gain in Perovskite Semiconductor Nanocrystals. *Nano Lett.* **2021**, *21* (18), 7831–7838.
- (110) Feng, L.; Wong, Z. J.; Ma, R. M.; Wang, Y.; Zhang, X. Single-mode laser by parity-time symmetry breaking. *Science* **2014**, *346* (6212), 972–975.
- (111) Hodaei, H.; Miri, M. A.; Heinrich, M.; Christodoulides, D. N.; Khajavikhan, M. Parity-time-symmetric microring lasers. *Science* **2014**, *346* (6212), 975–978.